Stability of respiratory-like droplets under evaporation

Carola Seyfert [1], Javier Rodríguez-Rodríguez [2,*], Detlef Lohse [1,†] and Alvaro Marin [1]

[1]*Physics of Fluids Group, Department of Science and Technology, Mesa + Institute, Max Planck Center for Complex Fluid Dynamics and J. M. Burgers Centre for Fluid Dynamics, University of Twente, 7500 AE Enschede, The Netherlands*

[2]*Departamento de Ingeniería Térmica y de Fluidos, Gregorio Millán Institute for Fluid Dynamics, Nanoscience and Industrial Mathematics, Universidad Carlos III de Madrid, 28911 Leganes, Spain*

Recent studies have shown that enveloped viruses contained in airborne respiratory droplets lose infectability fastest at intermediate ambient relative humidities H_r. However, the precise physicochemical mechanisms that generate such least-favorable conditions for the virus are not fully understood yet. Studying the evaporation dynamics of respiratory-like droplets in air experimentally and analytically, we reveal that at high H_r, the salt dissolved in respiratory drops inhibits their evaporation indefinitely. Conversely, at low H_r the drop evaporates leaving a porous solid residue, inside which virions may remain dormant for long times. We conclude that the optimal relative humidity for minimal infectability should coincide with droplets containing the maximum concentration of salt for longest periods of time.

I. INTRODUCTION

The recent COVID19 pandemic has revealed how little we know about the physical mechanisms that allow infectious agents to be transmitted through air [1,2]. Indeed, airborne pathogens like influenza viruses and corona viruses, but also bacterial agents like tuberculosis or legionellosis, can survive for hours or even days in exhaled droplets [3,4], depending on the environmental conditions. For instance, Influenza, an enveloped virus like the SARS-CoV-2, is typically transmitted more efficiently during the winter season (typically cold and dry) but also in rainy seasons in warmer climates (warm and wet) [5,6]. However, transmission efficiency is a very complex issue since it involves, besides physical aspects like the environmental conditions on the transmission route (air flows, humidities, and temperatures), biological ones (for example, the host's or recipient's immune system reaction to these environmental conditions). During airborne transmission, the virus is usually expelled from a host in droplets, through coughing, speaking, laughing, or simply breathing [7–11]. These water-based respiratory droplets contain, in addition to potential pathogens, a wide variety of salts, proteins and surfactants, the concentrations of which determine the salinity and pH of the solution. Previous empirical studies have shown that the relative humidity plays a significant role in the survival of airborne influenza viruses [12]. Assuming that a pathogen can survive longer in a water-based suspension at the right pH and salinity, one would expect that very dry conditions would certainly be very adverse for a pathogen. This seems to be the case for most bacteria, with only few exceptions [13].

---

*bubbles@ing.uc3m.es

†Also at Max Planck Institute for Dynamics and Self-Organization, 37077 Göttingen, Germany.

However, recent data have shown that viruses do not only survive at high relative humidities (H_r) but, contrary to intuition, also at extremely low ones, with a substantial decay in activity for intermediate H_r [14]. The precise values of such humidities vary for different studies [15–17], as do the proposed mechanisms for such a nonlinear dependence of the viral activity with H_r. These new findings modify substantially the picture that, until the outbreak of the current COVID19 pandemic, most experts had about respiratory droplets in air, based on that given by Wells in the 1930s [18,19]. In this picture, small respiratory droplets produced by sneezing, coughing, or speaking would quickly evaporate (and therefore thought to be less dangerous), while the large ones would follow ballistic trajectories and quickly hit the floor. Confidence in this picture led authorities over the globe to implement the six-foot distance rule to reduce the spread of COVID19. However, this picture has shown to be incomplete. Some good examples have been recently shown by direct numerical simulations (DNS) of aerosols [20,21], showing that the temperature and relative humidity field is rather heterogeneous within a puff containing respiratory droplets. This leads to a dramatic increase of the small droplets' lifetime, which can increase up to 150 times, and consequently the aerosol can be transported much further than initially expected. Neither this study nor any other of the recently published ones on the spread of infectious respiratory puffs (to our knowledge) have taken into account the effect of the dissolved solutes in the respiratory liquid combining models based on basic principles and experiments. However, the presence of solutes modifies the evaporation dynamics and, thus, has an impact on the settling and transportation of the drops, which differ from that of pure water ones [22–24].

In this work we explore the role that the dissolved solutes have on the inhibition of evaporation of airborne respiratory droplets and on the properties of the dry residue left upon evaporation. This is achieved by studying spherically shaped droplets semilevitating on superhydrophobic substrates with fractal-like microstructures [25]. This experimental method allows us to emulate the drying of exhaled aerosol droplets in a much more controlled way than in aerosol chambers and, more importantly, it permits us to retrieve the intact droplet nuclei (the dry remains) for analysis using scanning electron microscopy. Our experimental and analytical results address one of the key open questions in the problem of airborne disease transmission: what are the physicochemical mechanisms that lead to the inactivation of the virions while they are confined in a respiratory aerosolized droplet?

II. EXPERIMENTAL SETUP AND METHODOLOGY

We perform experiments using droplets of respiratory-like water-based solutions containing salt (9 g/l NaCl), protein (3 g/l dehydrated mucin from porcine stomach), and surfactants (0.5 g/l 1,2-Didodecanoyl-sn-glycero-3-phosphocholine, hereafter DPPC), as used in recent studies [14,17]. To understand the role of each of the components in the evaporation process, droplets in the microliter range are gently deposited on an omniphobic substrate with a fractal-like structure [25,26]. A standard vapour deposition protocol renders the substrate omniphobic, by depositing a layer of Fluoroctatrichlorosilane (FOTS) on top of the microfabricated structures. The substrates display a static contact angle of $\geqslant 155°$ for water droplets, and roll-off angles as low as $1.5°$.

The droplets employed contain either pure water as reference (high purity Milli-Q) or one of the following variations of the solutes: salt; salt and protein; salt, protein, and surfactant. The organic components are purchased from Sigma-Aldrich. We mix the solutions on a magnetic stirrer, with minimal heating, in a covered glass beaker to avoid evaporation of the solvent during the mixing. Salt and DPPC dissolve fairly quickly in water under stirring, the mucin takes roughly four times as long to fully dissolve. Before we do experiments, we vigorously mix the solutions on a vortex mixer, and also mix them on a magnetic stirrer again, to dissolve potentially precipitated mucin. After mixing, we centrifuge the solution for 10 minutes and extract the supernatant for our experiments. This last step ensures that no precipitated, agglomerated solids contaminate our experiments.

Droplets are left to evaporate under controlled conditions in a closed chamber, at constant room temperature and at different relative humidities ranging from 10% to 90%. We use a humidity
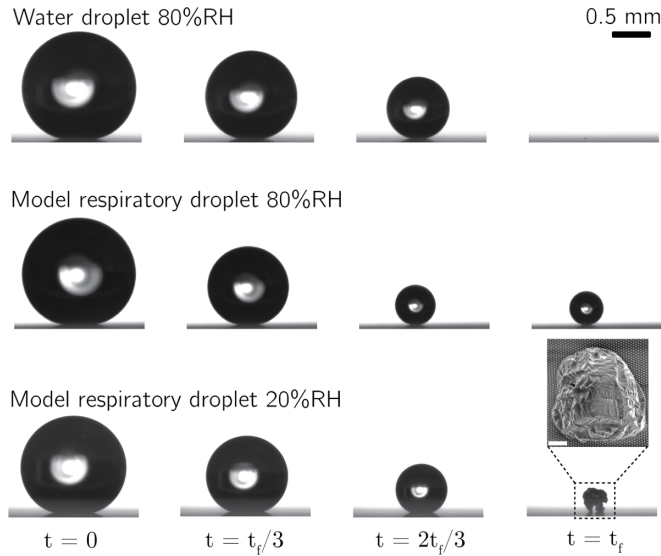
FIG. 1. Experimental images of evaporating droplets semilevitating on top of the superhydrophobic substrate. Time evolves increasing from the leftmost column $t = 0$ to the rightmost $t = t_f$, where t_f corresponds to the final evaporation time of a water droplet of approximately 3 μl at 80% RH for the first and second rows. Notably, while the water droplet completely evaporates (first row), the model respiratory droplet (second row) remains stable indefinitely. A model respiratory droplet evaporating at a relative humidity below the deliquescence limit (third row) leaves a solid but hollow residue, with a structure that depends on the relative amount of solutes initially dissolved and the evaporation process.

controller (HGC 30 from DataPhysics) to set the humidity in the chamber. To reach very low relative humidity values, we make use of the hygroscopic property of magnesium chloride and place "water traps" inside the chamber. These water traps are little vessels filled with dry magnesium chloride. This method leads to relative humidity values below 15%. The values for humidity and temperature within the chamber are monitored throughout all experiments.

We deposit a droplet on top of the omniphobic substrate with a threaded-plunger syringe and a tapered fused silica capillary (glass syringe from Hamilton, Model 1750 LT Threaded Plunger SYR, silica capillary from Polymicro Technologies). The nominal external diameter of the capillary is 360 μm. To avoid any sudden impact of the droplet on the substrate, we slowly increase its volume with the threaded plunger, while the droplet already touches the substrate. By retracting the capillary upwards, the droplet, now having reached volumes between 2 and 3 μl, detaches from the capillary and gently comes to rest on top of the substrate.

The omniphobic substrate is placed in between a CCD camera (Ximea MQ013MG-ON) and a light source. The droplet evolution is monitored from a side view using a long distance objective and a digital camera, from which the droplet volume is obtained as a function of time. Sequences of a typical experiment can be seen in Fig. 1, where the evaporation of a pure water droplet (first row) is compared to that of a model respiratory droplet containing salt, protein and surfactant (second row) at identical room temperature and relative humidity $H_r = 0.8$. Both droplets remain in a semilevitating state during the whole evaporation process, mimicking the process in an aerosol droplet in a quiescent atmosphere. Initially, both droplets evaporate at the same rate, but in the late stages the model respiratory droplet reaches a stationary size, while the water droplet evaporates completely as expected. The third row in Fig. 1 corresponds to a model respiratory droplet, in this case at a lower relative humidity than the previous ones $H_r = 0.2$, evaporating completely and leaving a solid residue.
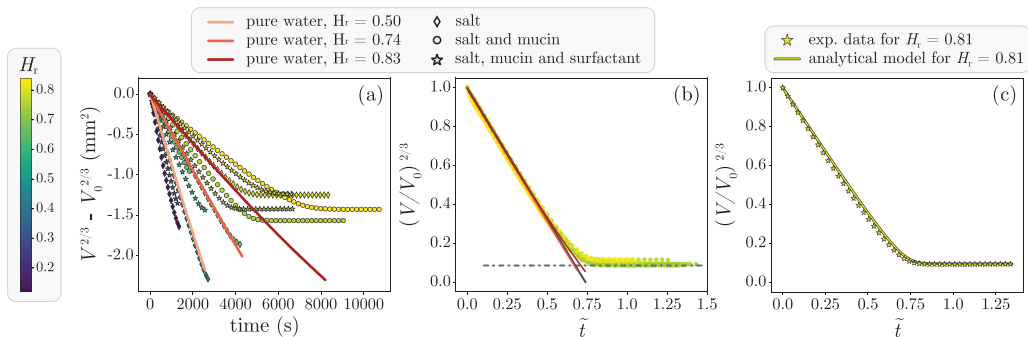
FIG. 2. (a) We show experimental curves of the droplet volume, as $V(t)^{2/3} - V_0^{2/3}$ (in mm^2), against time (in seconds) for a wide range of humidities. The colormap on the left indicates the relative humidity of each experiment [also in panels (b), (c)]. Composition of droplets is denoted by symbols (see the top legend). Additionally we show data for pure water droplets at three different relative humidities. For humidities smaller than $H_r = 0.75$, the experimental curves end when the drop has dissolved completely. (b) Normalized droplet volume, $(V(t)/V_0)^{2/3}$, against a dimensionless time $\tilde{t} = t/t_d$ with t_d being a diffusive evaporative timescale [27]. Using the normalization, which is independent of the droplet content, all experiments for $H_r \geqslant 0.75$ overlap. We furthermore plot two asymptotic limits of the evaporation process: the gray line denotes the linear model of volume reduction for pure water droplets. The dash-dotted green line indicates the prediction for the stable volume, based on the initial sodium chloride concentration in the droplets and the saturation concentration. (c) Comparison between experimental data and analytical model. The graph shows the normalized droplet volume $(V/V_0)^{2/3}$ with $V_0 = V(t = 0)$, against the normalized time $\tilde{t}$, as also shown in Fig. 2 of the main manuscript. As denoted in the legend, experimental data is shown with symbols, the analytical model with a line. The symbols for the experimental data were chosen in accordance with the other plots in this study. We present an example corresponding to a relative humidity 0.81. The model yields very good agreement with the experimental data for all the relative humidities explored, and in both limiting regimes: the diffusion-limited evaporation regime and the final stable volume.

III. EVAPORATION RATE OF RESPIRATORY-LIKE DROPLETS

Figure 2 shows this result in a quantitative way for all the liquid solutions and the full range of H_r employed in this study. As can be seen in dimensional form in Fig. 2(a), the volume of pure water droplets (red plots) decays in time as $V(t)^{2/3} - V_0^{2/3} \propto t$, i.e. it follows the well-known D^2-law for the full range of H_r explored. Here $V(t)$ is the droplet volume at a given time t and $V_0 = V(0)$. From these results we deduce that the process is diffusion-limited. However, any other solution containing sodium chloride will reach a stable diameter after a certain critical droplet size.

The first question is whether respiratory-like droplets will also evaporate following such a D^2-law or if any of their components (sodium chloride, mucin or surfactant) would alter their behavior, one way or another. To answer this question, we perform experiments at different humidities for three types of solutions: (a) sodium chloride (9 g/l), (b) sodium chloride and mucin (3 g/l), and (c) sodium chloride, mucin, and the surfactant DPPC (0.5 g/l). The results are also shown in Fig. 2(a), where we plot $V(t)^{2/3} - V_0^{2/3}$ against time.

We can see that, during a first stage of the evaporation process, the droplet volume evolves in time just like pure water droplets (solid lines), regardless of their composition (symbols). This is fairly well described by a simple model valid for pure water solutions, and has recently been shown for colloidal solutions [27]. Thus, we conclude that the early evaporation process is not affected by the composition of the droplet, regardless the relative humidity value.

Remarkably, the composition of the droplet, in combination with high relative humidities, starts to play an important role for the evaporation dynamics only at late times. Above a certain critical

relative humidity, all droplets containing salt reach a stable volume at a relative humidity of approximately 75%.

The final liquid volume depends on the composition, most strongly on the amount of sodium chloride initially introduced in the solution. The inhibition of evaporation (and hence, volume reduction and water loss) is a result of the vapor pressure dependence on the salt concentration of the solution. As the droplet loses water, the salt concentration increases and the vapor pressure decreases. The driving force of any evaporative process can be expressed as a difference in vapor pressures between the ambient and the liquid surface. Thus, this driving force becomes smaller as the salty droplet evaporates. As it turns out here, at 20°C, the minimum equilibrium vapor pressure of a stable sodium chloride solution, attained at saturation, corresponds to the vapor pressure of pure water at a relative humidity of approximately 75%. Consequently, all droplets containing sodium chloride being exposed to a relative humidity of 75% or above will evaporate only until they reach a salt concentration by which their vapor pressure matches that of pure water. We must point out that although in our experiments we find that the full-evaporation threshold consistently occurs at a relative humidity of 75%, other authors report that stable droplets can exist also at somewhat lower humidities [24]. We attribute this difference to the appearance of contact efflorescence, which precipitates the salt efflorescence due to the way our droplets rest on the hydrophobic substrates.

The consequences for respiratory aerosols are crucial: if this droplet were a respiratory aerosolized droplet in an environment at 20°C with high humidity (above its equilibrium relative humidity of 75%), this would result in a stable aerosolized droplet that would remain liquid indefinitely without drying. To understand and discuss the consequences of such a behavior, we proceed to model the system and compare it with our experimental results.

In the following, we model the evaporation of these droplets using the simplest physical model that reproduces the phenomena observed, such that it can be easily implemented in aerosol simulations [20]. We consider the evaporation of a droplet containing a nonvolatile solute that modifies the vapor pressure of the solution (in our case, sodium chloride dissolved in water).

If the evaporation is limited by diffusion, then the mass of solvent, m_w, in an isolated spherical drop of radius R changes with time as [28]

$$\frac{dm_w}{dt} = 4\pi R D \frac{p}{\mathcal{R}T} \ln\left(\frac{p - p_{v,a}}{p - p_{v,\infty}}\right), \tag{1}$$

where D the diffusivity of the vapor in air, p and T the air pressure and temperature, respectively, and $\mathcal{R}$ the ideal gas constant. Moreover, $p_{v,a}$ and $p_{v,\infty}$ are the vapor pressure at the droplet's surface and far away from it, respectively.

In the case of a sessile droplet with contact radius R_c and angle θ, this equation must be modified as pointed out in Ref. [29] to yield

$$\frac{dm_w}{dt} = \pi R_c f(\theta) D \frac{p}{\mathcal{R}T} \ln\left(\frac{p - p_{v,a}}{p - p_{v,\infty}}\right), \tag{2}$$

where $f(\theta)$ is a function of the contact angle,

$$f(\theta) = \frac{\sin\theta}{1 + \cos\theta} + 4 \int_0^\infty \frac{1 + \cosh(2\theta\tau)}{\sinh(2\pi\tau)} \tanh[(\pi - \theta)\tau]\, d\tau. \tag{3}$$

Besides the contact angle which we assume roughly constant during the evaporation process ($\theta \approx 150°$ in our experiments), an expression for the contact radius R_c is required [27],

$$R_c = \left(\frac{3V g(\theta)}{\pi}\right)^{1/3}. \tag{4}$$

Here, $g(\theta) = \sin^3\theta / [(2 + \cos\theta)(1 - \cos\theta)^2]$ and $V = (m_w + m_s)/\rho(\mu)$ is the drop volume. The density of the water-salt solution $\rho(\mu)$ is taken from Ref. [30]. It is a function of the salt weight

fraction of the solution,

$$\mu = \frac{m_s}{m_w + m_s}, \tag{5}$$

with m_s the mass of salt present in the drop (constant in time).

Since, even at 100% relative humidity, the water vapor pressure is much smaller than the atmospheric one, we can simplify Eq. (2) to

$$\frac{dm_w}{dt} = \pi R_c f(\theta) D\left(\frac{p_{v,\infty}}{\mathcal{R}T} - \frac{p_{v,a}}{\mathcal{R}T}\right). \tag{6}$$

We can further simplify this equation by defining $p_{v,\infty} = H_r p_v(T)$, where H_r is the relative humidity and $p_v(T)$ is the vapor pressure at a given temperature, which can be computed using Antoine's equation [20]. The vapor pressure of the water at the surface of the drop is given by $p_{v,a} = \chi_w p_v(T)$, where χ_w is the so-called water activity. Although it may be estimated as the molar fraction of water in the dissolution, in this work we take its value from an experimental investigation reported elsewhere [31], where this activity is provided as a function of the salt weight fraction of the solution, $\chi_w(\mu)$. Denoting by $c_s = p_v(T)/\mathcal{R}T$ the water vapor mass concentration in air at saturation conditions, we can finally write

$$\frac{dm_w}{dt} = \pi R_c f(\theta) D c_s (H_r - \chi_w). \tag{7}$$

Last, to compare the results of experiments with different relative humidity, it is convenient to define a timescale for the problem. To do so, we apply Eq. (7) to the first stage of the dissolution, where the salt concentration is small, $\mu \ll 1$. Consequently, $\chi_w \simeq 1$ and $\rho \simeq \rho_0$, with ρ_0 the density of pure water. In these conditions $m_w \approx \rho_0 V$ and we can write

$$\frac{dV}{dt} = \pi \left[\frac{3V g(\theta)}{\pi}\right]^{1/3} f(\theta) \frac{D c_s}{\rho_0} (H_r - \chi_w). \tag{8}$$

This equation can be integrated to yield

$$\left(\frac{V}{V_0}\right)^{2/3} - 1 = -f(\theta)\left(\frac{g(\theta)}{2}\right)^{1/3} \frac{t}{t_d} = -f(\theta)\left(\frac{g(\theta)}{2}\right)^{1/3} \widetilde{t}, \tag{9}$$

where $t_d = \rho_0 R_0^2/Dc_s(1 - H_r)$ is a diffusive evaporation timescale, $R_0 = (3V_0/4\pi)^{1/3}$ the volume-equivalent initial droplet radius and $\widetilde{t} = t/t_d$ is the dimensionless time. Equation (9) holds for early times $\widetilde{t} < 0.7$ and collapses the data as can be seen in Fig. 2.

An important consequence of Eq. (7) is that the drop stops dissolving, $dm_w/dt = 0$, when the vapor pressure at its surface becomes equal to that far away from the droplet, thus $\chi_w = H_r$. This means that respiratory droplets, which start from a water activity close to one, will not evaporate completely if the relative humidity is larger than the minimum water activity it can reach at saturation, $\chi_{w,\min} \approx 0.76$, this value corresponding to salt saturation conditions [32]. Notice that for relative humidities larger than the critical one, $H_r \gtrsim 0.75$, the droplet stops evaporating with a salt concentration smaller than the saturation one, as the condition $\chi_w = H_r$ is attained earlier in the evaporation process. Figure 2(b) shows the normalized experimental results, with the time re-scaled in line with the dimensional analysis of Eq. (7). The graph also includes the asymptotic volume predicted by Eq. (7) for $H_r = 0.75$. As can be seen, our results show an excellent agreement with the model for all solutions and environmental conditions [see also Fig. 2(c) for a more detailed comparison]. Note that extending our results to aerosol droplets (small enough so that the effect of the settling velocity is negligible in the evaporation rate) is trivial and would only involve a minor curve shift. In fact, the experimental model we present here reproduces the behavior of these small drops, which remain airborne for longer times. Finally, the model can be also applied to different temperatures by simply finding the right values for χ_w from the tables provided in the literature [32].
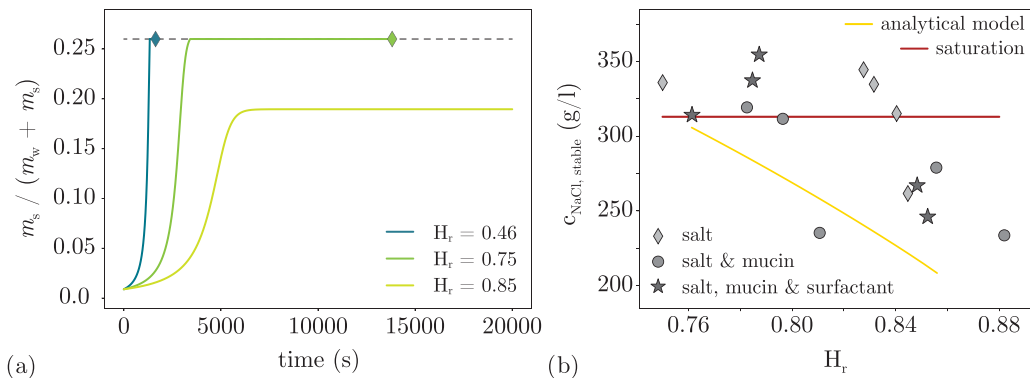
FIG. 3. (a) Time evolution, computed using our model, of the mass concentration of NaCl in a droplet with initial radius $R_0 = 0.7$ mm containing only this salt, for three different humidities. In those cases where the droplet dissolves completely, the diamond markers indicate the final evaporation time. The horizontal dashed line marks the salt saturation value: mass salt fraction 26%. (b) Concentration of sodium chloride in solution in stable liquid droplets. The mass of sodium chloride is computed based on the initial concentration in *solution*. The concentration $c_{NaCl,stable}$ denotes the mass of sodium chloride per unit volume in the stable drop. The red line in this plot corresponds to the saturation concentration at 20°C: 313 g/l. Note that this concentration is given as mass per volume of solution in a stable drop. The yellow line denotes the analytical model, discussed in the text. The droplets tend to stabilize at lower salt concentrations as the relative humidity increases.

IV. EVOLUTION OF THE SALT CONCENTRATION IN THE EVAPORATING DROPLET

Given the good agreement between the time evolution of the droplet volume predicted by our model and that measured experimentally, we proceed to use the model to determine the instantaneous salt concentration during the evaporation process. The evolution of this concentration is crucial to learn about the environment in which a virus, or any other pathogen within the droplet, needs to endure. In fact, while the drop is in liquid state, the presence of salt is the main responsible component for the inactivation of the virions contained in it [33]. Recent experiments report that this inactivation occurs at a rate proportional to the salt concentration [14]. Thus, being able to predict the time evolution of the salt concentration is instrumental in the formulation of any virus inactivation model.

In Fig. 3(a) we show the time evolution of the calculated salt mass fraction in the liquid phase for three drops of initial size $R_0 = 0.7$ mm (comparable to those shown in Fig. 1) at three different relative humidities, namely $Hr = 0.46, 0.75$ and 0.85. In the two first cases, since the humidity is below the deliquescence limit, the drop fully evaporates while in the third one the droplet reaches a stable volume in liquid state. When the relative humidity is well below the deliquescence limit (as for instance in the case $H_r = 0.46$), the salt mass concentration in the liquid grows rather quickly to the saturation value (around 0.26), which is maintained for a short time until all the liquid is gone (the instant indicated by a marker in the plot). Note that, once the saturation concentration is reached, an equilibrium between the evaporation rate and the salt precipitation leads to constant salt mass fraction in the liquid phase. In comparison, for the curve corresponding to a humidity close to the deliquescence limit ($H_r = 0.75$), the duration of the period in which the salt concentration is comparable to or equal to the saturation one is much longer. Finally, in the case well above deliquescence ($H_r = 0.85$) salt mass concentration takes much longer to rise to a level comparable to saturation, which is never achieved. The implications of these different behaviors for viral inactivation will be discussed later.

For completeness, we show in Fig. 3(b) the final salt mass concentration in the stable liquid drops resulting for humidities larger than the deliquescence limit, both measured experimentally and predicted with our model plus tabulated salt solution densities [30]. We can see that the final salt
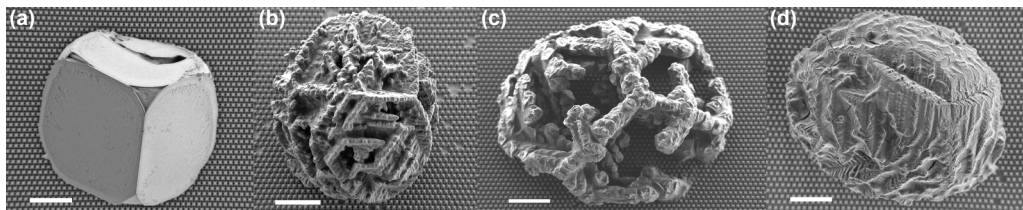
FIG. 4. Scanning electron micrographs taken from the remains of dried droplets containing (a) sodium chloride (initial droplet volume 3.5 μl), (b) sodium chloride and mucin (initial droplet volume 1.4 μl), and (c, d) sodium chloride, mucin and surfactant (respiratory-like droplets with initial volume 1.6 and 2.2 μl, respectively). All scale bars correspond to 100 μm. The micrographs are taken facing the superhydrophobic substrate [25,27] where the droplets are deposited.

concentration is, within experimental dispersion, identical regardless of whether the drop contains only salt or also contains mucin and/or surfactant.

As a final remark to this subsection we point out that, in our theoretical model, we impose that the salt concentration cannot be above the saturation limit (26% in mass fraction or 313 g/l at 20°C). This condition yields the most consistent comparison with our experiments. However, some experimental investigations reveal that free airborne droplets can temporarily reach metastable supersaturated salt concentrations [34]. Notice that, if needed, our mathematical model could easily be modified to account for this behavior by just extending the tables of water activity to concentrations above supersaturation.

V. DROPLET DRY-OUT AND RESULTING STRUCTURE

For relative humidities below 75%, the water completely evaporates and a dry object is left behind, often known in the literature as *droplet nucleus*. Interestingly, all droplets collapse into three-dimensional structures with a shape that strongly depends on its components, and to a lesser extent on the humidity. A great advantage of evaporating the droplets in such a controlled way is that we can analyze the intact remains under a scanning electron microscope. Figure 4 shows the remains of droplets with different contents. In all cases, the droplets are evaporated until they reach stability (for $H_r \geqslant 0.75$) and then they are slowly dried by reducing progressively the ambient humidity. Figure 4(a) shows the remains of a droplet containing only sodium chloride. The result is a single massive crystal-shaped remain. In Fig. 4(b) we observe the remains of a droplet containing salt and mucin, and in Figs. 4(c) and 4(d), salt, mucin, and surfactant. While the presence of protein and surfactants at such initial concentrations does not seem to affect the evaporation rate within our experimental measurements [see Fig. 2(b)], it strongly influences the final shape of the droplet nuclei. Salt crystallization is dramatically disturbed and several small-scale crystals are formed, nucleated all over the interface. Respiratory-like droplets (containing the three components) turn either into an open [Fig. 4(c)] or a closed structure, covered by a continuous layer of protein/surfactant as in Fig. 4(d). This structure, salt crystals coated by organic material, is consistent with that recently observed applying fluorescence microscopy to respiratory-like levitated droplets (and also to droplets with similar salt-protein compositions) [24]. Whenever salt and mucin are present, we always observe a "bone-like" structure made of sodium chloride crystals, coated by mucin protein and/or surfactant. The compactness of dried respiratory-like droplets is quite low, yielding rather holey structures. For instance, the estimated density of the dry residues showed in Fig. 4 are (a) 2016 kg/m^3, (b) 500 kg/m^3, (c) 305 kg/m^3, and (d) 420 kg/m^3 (see the Appendix). Given that the density of sodium chloride is 2170 kg/m^3, it is evident that the addition of mucin and the surfactant DPPC yields structures with a large void fraction that offer potential pockets where virions could remain protected in dried (or semidried) droplet residues. Such hollow structures are clearly observed also in the micrographs in Fig. 4 and it is consistent with recent

theoretical studies that predict their formation in spherical airborne droplets [35]. Interestingly, such dried shell microstructures would quickly rehydrate if the enviromental humidity is increased above the deliquescence limit ($H_r > 0.75$) due to the presence of salts [34,36]. Molecular dynamics simulations suggest that solid salt residues keep losing water for a time much longer than the one taken for the drop to evaporate, which may explain the rapid rehydration we observe [37,38].

VI. DISCUSSION

Our experimental and analytical results clearly show that the deliquescence limit establishes three different situations for a respiratory droplet containing pathogens, as others have recently hypothesized by different means [33]. The first situation occurs when the relative humidity is well below 75% ($H_r < 0.75$). The droplet dries out completely, leaving a dry object (droplet nucleus) behind. Recent research [13] indicates that enveloped viruses, like influenza [39] or SARS-CoV-2 [14], exhibit very slow viral inactivation rates in such dry remains as those shown in Fig. 4(c) or 4(d) and can, therefore, infect other individuals for longer times. Our model predicts (see Sec. IV and Fig. 3) that, when the humidity is well below deliquescence limit, the virions would spend comparatively little time exposed to salt in the solution, since the salt concentration changes quickly from the initial low values to crystallization, when the solvent evaporates completely. A very different situation would occur when the droplet finds itself in an environment around the deliquescence limit ($H_r \approx 0.75$). In such conditions, a respiratory droplet containing an active enveloped virus would remain for long times at a stable salt concentration close or even slightly higher than saturation, which would degrade fast its viral envelope and spike protein, and consequently result in a fast inactivation rate. While cell membranes in animals, plants and some bacteria have mechanisms to handle large salt concentrations [40], viral membranes do not have such a mechanism, and therefore are vulnerable to the damage that salt exerts on their envelop [33], and on the spike protein that allows the virus to bind to cells [41,42]. Indeed, salt concentration increases almost 3 orders of magnitude in such a droplet (well above the standard concentration in liquids in the human respiratory track), leading to an acceleration of the virus inactivation rate and making a droplet around the deliquescence limit a rather hostile environment for an enveloped virus. Finally, as the relative humidity further increases, a third situation emerges and a droplet would stabilize at larger volume and lower salt concentration. Moreover, the time taken for the drop to reach salt concentrations comparable to the stable one is longer than for a droplet close to deliquescence to reach saturation. We can conclude that an enveloped virus would find itself a longer time in a solution with mild salt concentrations when the relative humidity is above the deliquescence limit. Consequently, if we assume that there is indeed a correlation between the exposure to high salt concentration and the virus infectivity, then such virions should exhibit a slower inactivation rate and survive longer times.

These results give physical support to several studies that suggest that enveloped viruses have a higher tendency to survive at extreme values of relative humidity, either low or high [13,14,17,43], while their survival decreases to a minimum at intermediate values. Our results support empirical studies showing a dramatic extension of the predicted lifetime of respiratory droplets in humid environments and we provide an analytical model that could be easily implemented in state-of-the-art numerical simulations of aerosols [20,21]. Our model not only provides a simple and accurate description of the droplet evaporation rate during the whole process (from the D^2-law regime to the final volume stabilization), but also of the time evolution of the salt concentration that a virus would be exposed to. Combined with estimations of the viral decay in respiratory droplets (due to the presence of salt), such numerical models would enable, in the near future, the accurate estimation of the percentage of active virions contained in aerosols as well as the prediction of their spreading in different situations. Last but not least, the experimental approach proposed here allows us to explore the structure of the dried residue using advanced microscopy techniques. Such residues have a large void fraction, offering locations where virions can settle upon the evaporation of the liquid.

TABLE I. Estimated properties of the dry residues shown in Figs. 3(b)–3(d).

Case	R_{res} (μm)	c_{nv} (g/l)	V_0 (μl)	ρ_{res} (kg/m^3)
b	400	12	1.4	500
c	500	12.5	1.6	305
d	500	12.5	2.2	420

APPENDIX: ESTIMATION OF THE DENSITY OF THE DRY RESIDUE

We estimate the average density of the residues shown in Fig. 4 by assuming their shape is a cube [Fig. 4(a)] or a sphere [Figs. 4(b)–4(d)].

In the first case (a), we can estimate a cube side of $L = 250$ μm, which gives an apparent volume for the residue of $V_{res} = 0.0157$ mm$^3 = 0.0157$ μl. The initial drop volume (3.5 μl) contained 9 g/l of sodium chloride. Therefore, the density of the cube is $\rho_{res} = 3.5 \times 9$ μg/0.0157 μl = 2016 g/l = 2016 kg/m^3.

As for the objects in Figs. 4(b)–4(d), we assume them spheres of radius R_{res}. Besides the salt, they have 3 g/l of the protein mucin and, in Figs. 4(c) and 4(d), also 0.5 g/l of surfactant. We denote c_{nv} to this mass concentration of nonvolatiles. Finally, calling V_0 to the initial liquid volume of the drop, we have that the estimated density of the residue is

$$\rho_{res} = \frac{c_{nv}V_0}{\frac{4}{3}\pi R_{res}^3}. \tag{A1}$$

We report these values, and the resulting estimated densities, in Table I. Note that, even in the conservative case where these residues where semispheres, still its density would be less than half that of sodium chloride, which proves their large void fraction (consistently with the images seen in Fig. 3).

---

[1] C. C. Wang, K. A. Prather, J. Sznitman, J. L. Jiménez, S. S. Lakdawala, Z. Tufekci, and L. C. Marr, Airborne transmission of respiratory viruses, Science **373**, eadb9149 (2021).

[2] W. C. K. Poon, A. T. Brown, S. O. L. Direito, D. J. M. Hodgson, L. Le Nagard, A. Lips, C. E. MacPhee, D. Marenduzzo, J. R. Royer, A. F. Silva, J. H. J. Thijssen, and S. Titmuss, Soft matter science and the covid-19 pandemic, Soft Matter **16**, 8310 (2020).

[3] C. Geller, M. Varbanov, and R. E. Duval, Human coronaviruses: Insights into environmental resistance and its influence on the development of new antiseptic strategies, Viruses **4**, 3044 (2012).

[4] J. W. Tang, The effect of environmental parameters on the survival of airborne infectious agents, J. R. Soc., Interface **6**, S737 (2009).

[5] J. D. Tamerius, J. Shaman, W. J. Alonso, K. Bloom-Feshbach, C. K. Uejio, A. Comrie, and C. Viboud, Environmental predictors of seasonal influenza epidemics across temperate and tropical climates, PLoS Pathog. **9**, e1003194 (2013).

[6] A. Božič and M. Kanduč, Relative humidity in droplet and airborne transmission of disease, J. Biol. Phys. **47**, 1 (2021).

[7] L. Morawska, G. Johnson, Z. Ristovski, M. Hargreaves, K. Mengersen, S. Corbett, C. Chao, Y. Li, and D. Katoshevski, Size distribution and sites of origin of droplets expelled from the human respiratory tract during expiratory activities, J. Aerosol Sci. **40**, 256 (2009).

[8] L. Bourouiba, E. Dehandschoewercker, and J. W. Bush, Violent expiratory events: On coughing and sneezing, J. Fluid Mech. **745**, 537 (2014).

[9] L. Bourouiba, The fluid dynamics of disease transmission, Annu. Rev. Fluid Mech. **53**, 473 (2021).

[10] L. Morawska and D. K. Milton, It is time to address airborne transmission of coronavirus disease 2019 (covid-19), Clin. Infect. Dis. **71**, 2311 (2020).

[11] S. Asadi, N. Bouvier, A. S. Wexler, and W. D. Ristenpart, The coronavirus pandemic and aerosols: Does COVID-19 transmit via expiratory particles? Aerosol Sci. Technol. **54**, 635 (2020).

[12] K. A. Kormuth, K. Lin, A. J. Prussin, E. P. Vejerano, A. J. Tiwari, S. S. Cox, M. M. Myerburg, S. S. Lakdawala, and L. C. Marr, Influenza virus infectivity is retained in aerosols and droplets independent of relative humidity, J. Infect. Dis. **218**, 739 (2018).

[13] K. Lin, C. R. Schulte, and L. C. Marr, Survival of MS2 and ϕ6 viruses in droplets as a function of relative humidity, pH, and salt, protein, and surfactant concentrations, PLoS One **15**, 1 (2020).

[14] D. H. Morris, K. C. H. Yinda, A. Gamble, F. W. Rossine, Q. Huang, T. Bushmaker, R. J. Fischer, M. J. Matson, N. van Doremalen, P. J. Vikesland *et al.*, Mechanistic theory predicts the effects of temperature and humidity on inactivation of SARS-CoV-2 and other enveloped viruses, eLife **10**, 1 (2021).

[15] F. Schaffer, M. Soergel, and D. Straube, Survival of airborne influenza virus: Effects of propagating host, relative humidity, and composition of spray fluids, Arch. Virol. **51**, 263 (1976).

[16] J. Benbough, Some factors affecting the survival of airborne viruses, J. Gen. Virol. **10**, 209 (1971).

[17] E. P. Vejerano and L. C. Marr, Physicochemical characteristics of evaporating respiratory fluid droplets, J. R. Soc., Interface **15**, 20170939 (2018).

[18] W. F. Wells, On air-borne infection: Study II. Droplets and droplet nuclei, Am. J. Epidemiol. **20**, 611 (1934).

[19] W. F. Wells and M. W. Wells, Air-borne infection, JAMA, J. Am. Med. Assoc. **107**, 1698 (1936).

[20] K. L. Chong, C. S. Ng, N. Hori, R. Yang, R. Verzicco, and D. Lohse, Extended Lifetime of Respiratory Droplets in a Turbulent Vapor Puff and its Implications on Airborne Disease Transmission, Phys. Rev. Lett. **126**, 034502 (2021).

[21] C. S. Ng, K. L. Chong, R. Yang, M. Li, R. Verzicco, and D. Lohse, Growth of respiratory droplets in cold and humid air, Phys. Rev. Fluids **6**, 054303 (2021).

[22] R. R. Netz, Mechanisms of airborne infection via evaporating and sedimenting droplets produced by speaking, J. Phys. Chem. B **124**, 7093 (2020).

[23] J. S. Walker, J. Archer, G. F. K. A., S. E. S. Michel, B. R. Bzdek, and J. P. Reid, Accurate representations of the microphysical processes occurring during the transport of exhaled aerosols and droplets, ACS Cent. Sci. **7**, 200 (2021).

[24] E. Huynh, A. Olinger, D. Woolley, R. K. Kohli, J. M. Choczynski, J. F. Davies, K. Lin, L. C. Marr, and R. D. Davis, Evidence for a semisolid phase state of aerosols and droplets relevant to the airborne and surface survival of pathogens, Proc. Natl. Acad. Sci. USA **119**, e2109750119 (2022).

[25] E. J. Berenschot, H. V. Jansen, and N. R. Tas, Fabrication of 3D fractal structures using nanoscale anisotropic etching of single crystalline silicon, J. Micromech. Microeng. **23**, 055024 (2013).

[26] J. W. Berenschot, R. M. Tiggelaar, J. Geerlings, J. G. E. Gardeniers, N. R. Tas, M. Malankowska, M. P. Pina, and R. Mallada, 3D-fractal engineering based on oxide-only corner lithography, in *Proceedings of the Symposium on Design, Test, Integration and Packaging of MEMS/MOEMS (DTIP)* (2016), pp. 1–4.

[27] C. Seyfert, E. J. W. Berenschot, N. R. Tas, A. Susarrey-Arce, and A. Marin, Evaporation-driven colloidal cluster assembly using droplets on superhydrophobic fractal-like structures, Soft Matter **17**, 506 (2021).

[28] X. Xie, Y. Li, A. T. Y. Chwang, P. L. Ho, and W. H. Seto, Extended lifetime of respiratory droplets in a turbulent vapor puff and its implications on airborne disease transmission, Indoor Air **17**, 211 (2007).

[29] Y. O. Popov, Evaporative deposition patterns: Spatial dimensions of the deposit, Phys. Rev. E **71**, 036313 (2005).

[30] D. R. Lide *et al.*, *CRC Handbook of Chemistry and Physics, Internet Edition* (CRC Press, Boca Raton, FL, 2005).

[31] C. N. Papela and P. J. Dunlop, A re-examination of the vapour pressures of aqueous sodium chloride solutions at 25ºC, J. Chem. Thermodyn. **4**, 255 (1972).

[32] A. Apelblat and E. Korin, The vapour pressures of saturated aqueous solutions of sodium chloride, sodium bromide, sodium nitrate, sodium nitrite, potassium iodate, and rubidium chloride at temperatures from 227 K to 323 K, J. Chem. Thermodyn. **30**, 59 (1998).

[33] W. Yang and L. C. Marr, Mechanisms by which ambient humidity may affect viruses in aerosols, Appl. Env. Microbiol. **78**, 6781 (2012).

[34] F. Gregson, J. Robinson, R. Miles, C. Royall, and J. Reid, Drying kinetics of salt solution droplets: Water evaporation rates and crystallization, J. Phys. Chem. B **123**, 266 (2019).

[35] M. Rezaei and R. R. Netz, Water evaporation from solute-containing aerosol droplets: Effects of internal concentration and diffusivity profiles and onset of crust formation, Phys. Fluids **33**, 091901 (2021).

[36] A. P. Olsen, R. C. Flagan, and J. A. Kornfield, Single-particle levitation system for automated study of homogeneous solute nucleation, Rev. Sci. Instrum. **77**, 073901 (2006).

[37] M. Mucha and P. Jungwirth, Salt crystallization from an evaporating aqueous solution by molecular dynamics simulations, J. Phys. Chem. B **107**, 8271 (2003).

[38] D. Chakraborty and G. N. Patey, How crystals nucleate and grow in aqueous NaCl solution, J. Phys. Chem. Lett. **4**, 573 (2013).

[39] S. Asadi, N. G. ben Hnia, R. S. Barre, A. S. Wexler, W. D. Ristenpart, and N. M. Bouvier, Influenza A virus is transmissible via aerosolized fomites, Nat. Commun. **11**, 4062 (2020).

[40] C. M. Baumgarten and J. J. Feher, Chapter 16—Osmosis and Regulation of Cell Volume, in *Cell Physiology Source Book (4th Edition)*, edited by N. Sperelakis (Academic Press, San Diego, CA, 2012), pp. 261–301.

[41] R. Amaro, J. Stone, T. Miller, L. Chong, A. Ramanathan, and A. Mulholland, #covidisairborne: Ai-enabled multiscale computational microscopy of delta SARS-COV-2 in a respiratory aerosol, in *Proceedings of the International Conference for High Performance Computing, Networking, Storage, and Analysis* (2021).

[42] C. Zimmer and J. Corum, The coronavirus in a tiny drop, in The New York Times (Dec. 1, 2021), https://www.nytimes.com/interactive/2021/12/01/science/coronavirus-aerosol-simulation.html.

[43] K. Lin and L. C. Marr, Humidity-dependent decay of viruses, but not bacteria, in aerosols and droplets follows disinfection kinetics, Environ. Sci. Technol. **54**, 1024 (2020).